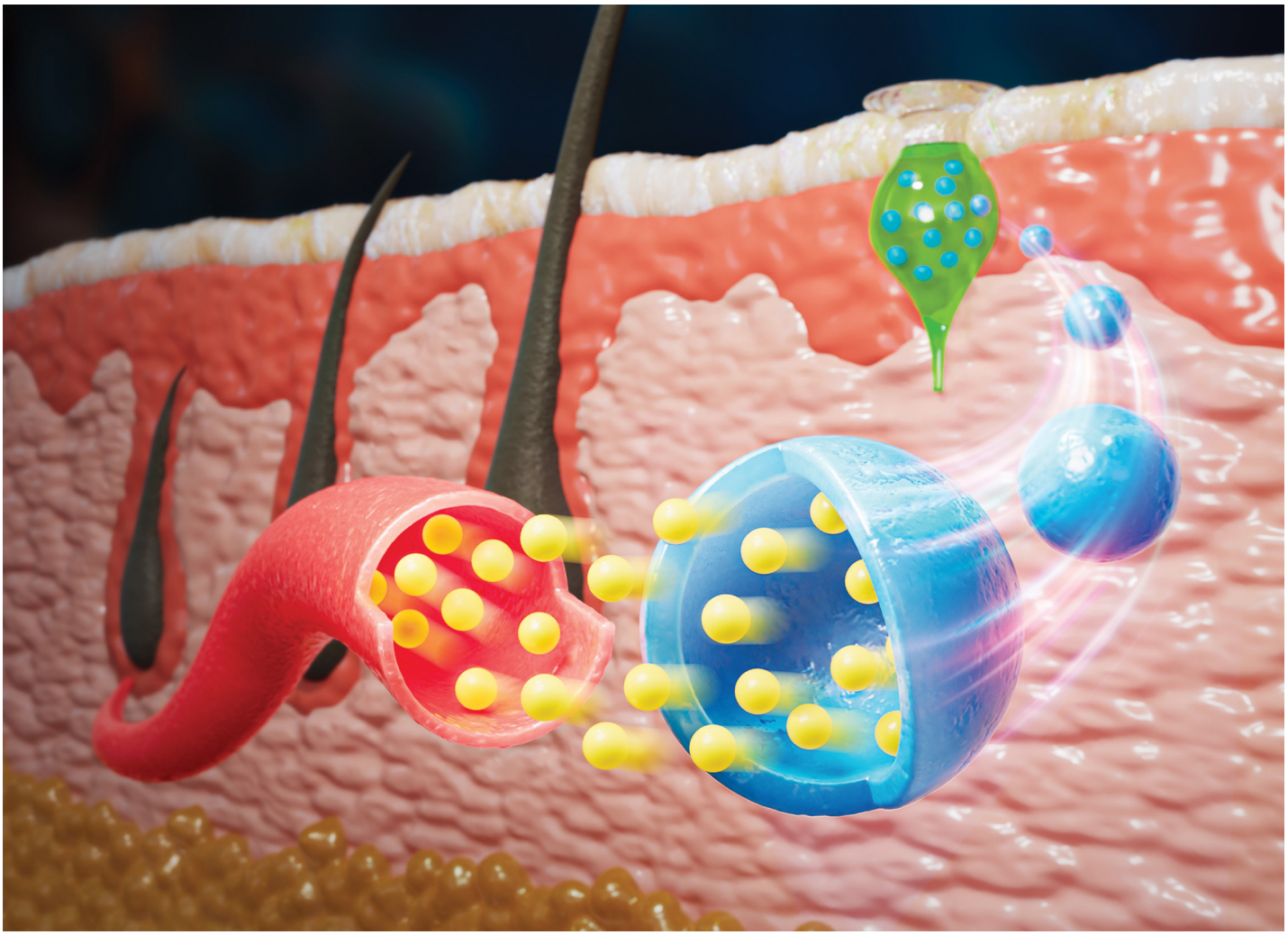

Showcasing research from Professor Hyungil Jung's laboratory, Department of Biotechnology, Yonsei University, Republic of Korea and TOPADUR Pharma AG, Switzerland.

Patient-convenient long-term alopecia treatment *via* PLGA microsphere-loaded candlelit microneedles

Androgenetic alopecia (AGA) causes progressive hair loss and psychological distress. Existing treatments have low bioavailability and side effects. This study introduces candlelit microneedles (CMNs) combined with PLGA microspheres encapsulating the nitric oxide-releasing vasodilator TOP-M119 for sustained delivery. CMNs overcome hair related application issues without adhesive patches. *In vivo* results show enhanced hair growth and reduced dosing frequency, suggesting improved efficacy and patient compliance over conventional therapies.

Image reproduced by permission of Hyungil Jung, Reto Naef from *J. Mater. Chem. B*, 2025, **13**, 5789.

As featured in:

See Reto Naef, Hyungil Jung *et al.*, *J. Mater. Chem. B*, 2025, **13**, 5789.

ROYAL SOCIETY OF CHEMISTRY

rsc.li/materials-b

Registered charity number: 207890

Journal of Materials Chemistry B

ROYAL SOCIETY OF CHEMISTRY

PAPER

View Article Online
View Journal | View Issue

Cite this: J. Mater. Chem. B, 2025, 13, 5789

Patient-convenient long-term alopecia treatment *via* PLGA microsphere-loaded candlelit microneedles†

Jiwoo Shin,[a] Sung min Cho,[a] Youseong Kim,[a] Geonwoo Kang,[b] Tobias Braun,[c] Hermann Tenor,[c] Christian Ludin,[c] Reto Naef*[c] and Hyungil Jung *[ab]

Received 17th January 2025,
Accepted 10th March 2025

DOI: 10.1039/d5tb00118h

rsc.li/materials-b

Androgenetic alopecia (AGA) is characterized by chronic and progressive hair loss, with associated psychological factors intensifying the impact on patients. Current treatments, such as oral finasteride and topical minoxidil, have low bioavailability and numerous side effects. Dissolvable microneedles (DMNs) provide a promising alternative for drug delivery. However, the presence of hair on the scalp often hinders their insertions and adhesion. Thus, candlelit microneedles (CMNs) have been developed to improve insertion and drug delivery without the use of adhesive patches. In this study, CMNs were combined with poly lactic-*co*-glycolic acid (PLGA) microspheres encapsulating the NO-releasing PDE5 inhibitor TOP-M119 (M119), a potent vasodilator promoting hair growth, for sustained drug release. When delivered *via* the CMN, it bypasses the challenges posed by hair on the scalp. The CMN system with PLGA microspheres resulted in substantial hair growth and reduced application frequency *in vivo*. This indicates that it may be a more effective treatment for alopecia than conventional methods. Furthermore, the reduced application frequency may result in better patient compliance.

Introduction

Androgenetic alopecia (AGA) is a chronic and progressive hair loss disorder caused by dihydrotestosterone, converted from testosterone by 5α-reductase, leading to follicular cell apoptosis.[1–3] Psychological factors may also affect the severity of AGA, as most patients with alopecia suffer from impairments in psychological well-being, self-esteem, and other psychological comorbidities.[4] Although AGA does not directly threaten physiological health, it may result in psychological effects leading to high levels of anxiety and depressions.[4,5]

Proposed treatments for alopecia include two United States Food and Drug Administration-approved drugs: oral finasteride and topical minoxidil.[6,7] Patients taking these drugs have reported significant hair regrowth and improvement.[3] Although drugs can ease the symptoms of alopecia, they have several side effects and limitations in administration methods. The orally administered finasteride has low bioavailability, owing to the lack of gastrointestinal tract stability, with the possibility of erectile dysfunction in men.[8–10] The topical administration of minoxidil has low efficacy for drug delivery because the stratum corneum impairs transdermal delivery. Furthermore, the potential adverse effects of this drug include hypertrichosis, postural hypertension, and edema.[11,12] These limitations necessitate the development of methods that can overcome the challenges associated with conventional drug administration.[13]

Microneedles (MNs) are a minimally invasive transdermal and intradermal drug delivery system that bypasses the stratum corneum.[14] Dissolvable microneedles (DMNs), a subtype of MN, have been widely utilized to overcome the challenges associated with traditional drug delivery.[15] DMNs are fabricated by mixing drugs with biodegradable polymers, allowing transdermal drug delivery *via* penetration, followed by dissolution in the stratum corneum.[16,17] Treatment of alopecia may take several months,[18] during which continuous hair growth can act as an additional barrier during this period, hindering the insertion of DMNs to the scalp. Additionally, hair makes it challenging to use traditional adhesive patch DMNs that provide firm attachment to the skin during transdermal drug delivery.

Kim *et al.*[19] introduced candlelit microneedles (CMNs), a type of DMN with a distinct curvature structure and a spring force applicator without an adhesive patch. CMNs have been shown to overcome the insertion limits of DMNs, owing to their geometrical feature that interlocks with the scalp and resists

[a] Department of Biotechnology, Yonsei University, 50 Yonsei-ro, Seodaemun-gu, Seoul, 03722, Republic of Korea. E-mail: hijung@yonsei.ac.kr
[b] JUVIC Inc., 272 Digital-ro, Guro-gu, Seoul, 08389, Republic of Korea
[c] TOPADUR Pharma AG, Grabenstrasse 11A, 8952 Schlieren, Switzerland. E-mail: reto.naef@topadur.com

† Electronic supplementary information (ESI) available. See DOI: https://doi.org/10.1039/d5tb00118h

extraction after insertion.[20] In addition, a spring force applicator was used for CMN insertion into the scalp, achieving both insertion and maintenance of the insertion state without employing an adhesive patch.[19] Although CMNs and the use of an applicator greatly increased drug delivery and insertion quality in previous studies, it was not applied to an area with hair, as the animal models used were shaved for observation of hair growth. In addition, frequent applications were required, which can significantly hinder patient compliance during treatment. A previous study used CMN applications once every two days, resulting in 10 administrations over 21 days.[19] As patient noncompliance is a major issue in healthcare, a method that simultaneously improves patient compliance and drug efficacy is required.

One way to facilitate patient compliance during alopecia treatment is sustained drug release over a long period, allowing full drug delivery with minimal administration. Poly lactic-*co*-glycolic acid (PLGA), a biodegradable polymer, is widely used as a drug delivery agent.[21] PLGA hydrolyzes into nontoxic lactic acid and glycolic acid; lactic acid has therapeutic effects against alopecia.[22] Thus, it shows excellent potential applicability in DMN utilization. Lin *et al.*[23] incorporated PLGA microspheres with conventional DMN for the long-acting release of minoxidil to treat alopecia, revealing an increase in patient compliance. However, previous studies on CMN and PLGA-incorporated DMN have not addressed the need for a system that works effectively in the presence of hair, as experiments were conducted on shaved animal models for hair growth observation. Therefore, a CMN that bypasses the limitations of DMNs and enhances patient compliance through PLGA-assisted drug delivery on hairy skin is required for the clinical application of long-term alopecia treatment.

In this study, a drug delivery method utilizing PLGA microspheres and CMN administration was introduced for effective alopecia treatment that also facilitates patient compliance. The efficacy of this method was further evaluated using an unshaven mouse model. We utilized the previously described NO-releasing PDE5 inhibitor TOP-M119 (M119), a superior vasodilator shown to increase hair growth *via* increased local blood flow caused by soluble guanylate cyclase stimulation and PDE-5 inhibition.[19] The encapsulation of M119 into PLGA microspheres enabled its sustained release, which markedly reduced the number of CMN administrations required. This ultimately increases drug efficacy and patient compliance. We successfully delivered M119-encapsulating PLGA microspheres into the skin using CMNs, which bypassed the growing hair barrier after administration. *In vitro* analyses elucidated the release profile of PLGA microspheres and the physical capabilities of CMNs. Optical coherence tomography (OCT) and fluorescence imaging were used to confirm the insertion of CMNs. Additionally, we evaluated the effectiveness of M119-encapsulating PLGA microsphere CMNs (MP-CMNs) *in vivo* by comparing the hair growth in 7-week-old C57BL/6 male mice. MP-CMNs were successfully administered to both shaven and hairy mouse skin, whereas conventional cone-shaped DMNs were less effective on hairy mouse skin. After 28 days, the application of MP-CMNs showed similar hair growth to that observed after 14 topical applications of minoxidil. Additionally, we demonstrated that MP-CMNs were successfully administered to hairy skin by inserting a second MP-CMN into the hair-grown skin. This study demonstrates that MP-CMNs provide a more convenient and potentially more effective treatment for alopecia than conventional methods, as they require fewer applications and accommodate continuous hair growth during treatment.

Results and discussion

Schematic conceptualization of MP-CMNs for alopecia treatment

A schematic of the MP-CMN-targeting alopecia treatment is shown in Fig. 1. As shown in Fig. 1(A), MP-CMNs were inserted using a spring-loaded applicator that drove the MP-CMN array using the elastic force of the spring. Each CMN in the MP-CMN array contained an M119-encapsulating PLGA microsphere located at the center of the microneedle. The MP-CMN subsequently dissolved to release PLGA microspheres which release the encapsulated M119. Adhesive patches were not required for fixation of the array on the skin post-insertion, as MP-CMN dissolution does not require prolonged attachment of the microneedle array. Also, geometries with a contoured surface allow microneedles to lock into skin after insertion, preventing the microneedle getting pushed out by skin resilience and tension.[24,25] This allows for short and concise insertion and removal of patches. Therefore, enhanced patient compliance might be achieved with MP-CMNs due to its capability of rapidly dissolving and releasing PLGA microspheres inside the skin for dissolution over 28 days. Hair growth was induced *via* M119, a dual-mode of action drug that inhibits PDE5 and promotes nitric oxide (NO) release, drastically enhancing cyclic guanosine monophosphate concentration (Fig. 1(B)).[19]

Fabrication and characteristics of PLGA microspheres and MP-CMN

M119-encapsulating PLGA microspheres were produced using 200 mg of PLGA with a lactide-to-glycolide ratio of 50 : 50 and 10 mg of M119. As shown in Fig. 2(A), nonporous and smooth-surfaced PLGA microspheres with an average particle size of 4.36 μm ± 0.05 μm were fabricated. The fabricated PLGA microspheres continually released M119 over 29 days, achieving one month of drug delivery term (Fig. 2(B)). The final release profile was 88.16 ± 5.62% on day 29, ensuring that most of the M119 was released from the PLGA microsphere once dissolved in the simulated interstitial fluid.

M119-encapsulating PLGA microspheres were further loaded onto the CMN, enabling transdermal drug delivery into the scalp. The MP-CMN comprised three distinct layers: the base, M119-encapsulating layer, and tip. Each layer was fabricated in three main steps: primary, secondary, and tertiary (with centrifugation) dispensing for base, drug-encapsulating, and tip layer formation, respectively (Fig. 2(C)). The base layer was prepared by dispensing a hyaluronic acid (HA) solution

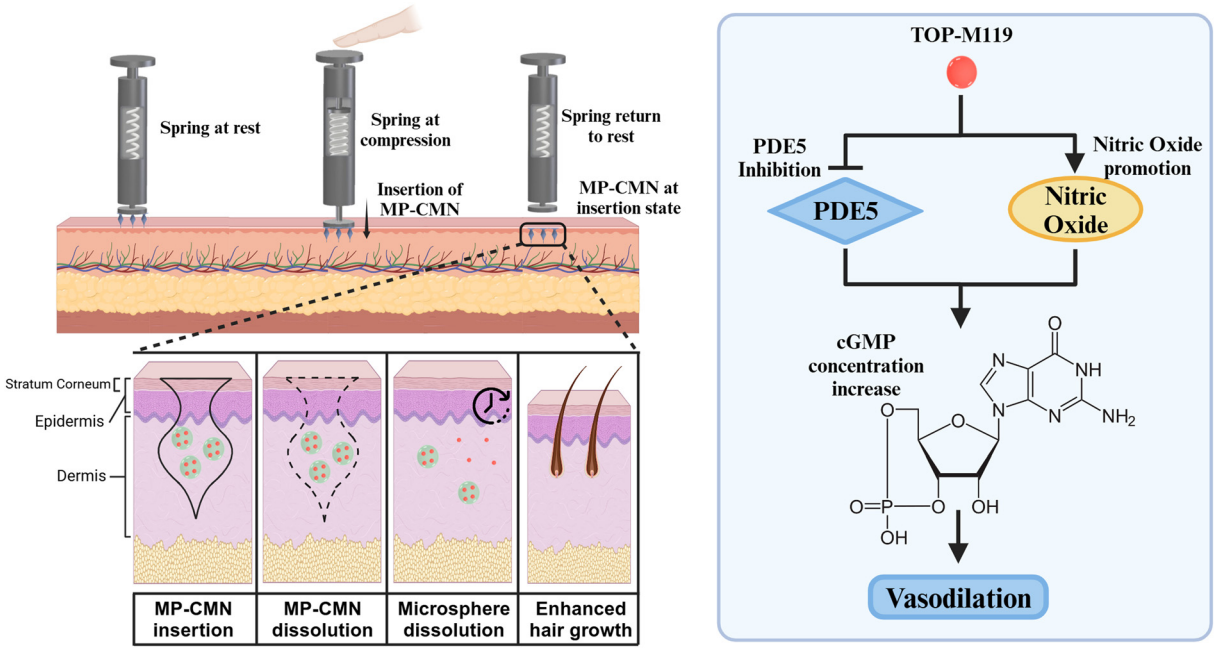

Fig. 1 (A) Schematic representation of MP-CMN insertion using spring force application and mode of action for sustained M119 release after skin insertion. (B) Schematic representation of the dual-mode of action NO-releasing PDE5 inhibitor M119 resulting in vasodilation.

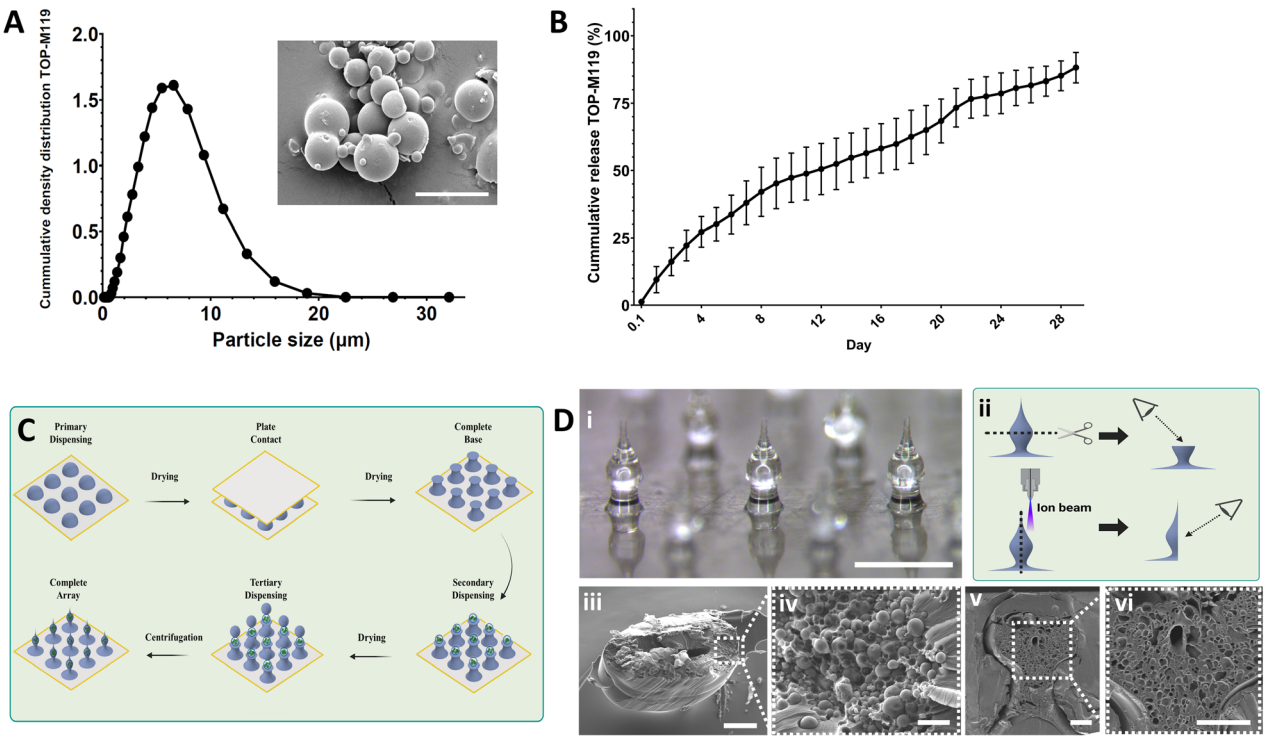

Fig. 2 (A) SEM image of M119-encapsulating PLGA microspheres and the log cumulative density distribution of particle sizes (scale bar: 10 μm). (B) Cumulative release profile of M119 from PLGA microspheres in simulated interstitial fluid, as measured from day 0.1 to 29 (n = 6). (C) Schematic representation of MP-CMN fabrication steps. (D) (i) Bright field microscopy of MP-CMN (scale bar: 1000 μm). (ii) Schematic image of horizontal mechanical cut and vertical ion beam cut MP-CMN and observation of the cross section. (iii) Surface morphology of an MP-CMN cross section, as captured using SEM (scale bar: 100 μm). (iv) Magnification of the sectional cut for PLGA microsphere observation (scale bar: 10 μm). (v) Surface morphology of a MP-CMN cross section, after ion beam cut, as captured using SEM (scale bar: 100 μm). (vi) Magnification of the ion beam sectional cut for PLGA microsphere observation (scale bar: 10 μm).

onto a polyurethane film, which was pressed with a plate and dried to create a base layer resembling a hyperboloid shape. The distance between the polyurethane film and pressing plate was 250 μm. Therefore, the produced base layer was also 250 μm in height. The hyperboloid-shaped base layer supported the M119-encapsulating and tip layers, providing an inclination during drug delivery in the case of incomplete insertion of the MP-CMN into the skin. The base layer contained no drug; therefore, it did not affect the delivery efficacy in the case of incomplete insertion. This ensured safety for MP-CMN applications, as drug delivery success was dependent on the insertion of a drug-encapsulating layer located on top of the base layer. The M119-encapsulating layer was prepared by dispensing and drying a mixture of M119-encapsulating PLGA microspheres and HA on top of the base layer.

The tip layer was prepared by dispensing an HA solution on top of the M119-encapsulating layer, followed by centrifugation for shaping. During centrifugation, the dispensed HA solution was dried and extended to form a microneedle tip, resulting in MP-CMN with a streamlined conformation. The sharp end of the tip layer enhanced the insertion efficiency of MP-CMN during administration.

The resulting MP-CMN array was fabricated as shown in Fig. 2(D)-(i). The final MP-CMN array height was approximately 1000 μm, sufficient for adherence to hair follicle cells and drug delivery to dermal papilla cells.[19] As most MP-CMNs are produced with HA, the dissolution of microneedles occurs quickly, due to the high solubility.[26] Thus, PLGA microspheres remain in the skin tissue. SEM was used to visualize the sectionally cut surface of the MP-CMN, revealing the PLGA microspheres within. Fig. 2(D)-(ii) shows a schematic of the MP-CMN horizontally cut at the core layer, which was viewed under SEM for PLGA microsphere observation. Fig. 2(D)-(iii) and (iv) show the inside of the MP-CMN after cutting it horizontally at the core layer, which splits the core layer and reveals MP-CMN content. While Fig. 2(D)-(v) and (vi) show the MP-CMN after vertical ion beam cutting from the microneedle tip to bottom, showing microspheres at the core part of the MP-CMNs. This showed scattered PLGA microspheres, indicating that MP-CMN contains PLGA microspheres without perforation or breaking of the original structure, thereby securing M119 content even after fabrication. This structure of MP-CMN and PLGA microspheres allows for the delivery of M119 into the skin as MP-CMN is dissolved, followed by the gradual degradation of PLGA microspheres for sustained drug release. Overall, the incorporation of PLGA microspheres into microneedles did not modify their physical structure.

Insertion analysis of MP-CMN arrays into pig cadaver skin

After the MP-CMN were fabricated, their skin-penetrating capability was tested *in vitro* using animal skin tissue. The mechanical strength of the MP-CMNs was first measured to analyze the maximum force that each MP-CMN could withstand before breakage. As shown in Fig. 3(A), a single MP-CMN withstood 2.37 ± 1.23 N of pressure force before breaking, which is sufficient for insertion into skin with a similar shape.[27] Although a single MP-CMN could withstand the physical force required for skin penetration, the number of microneedles on a single patch also determined the insertion quality. Pig cadaver skin was selected because its histological and physiological properties are similar to those of human skin, making it a good model for human skin permeability.[28] To observe the successful insertion of our CMN array, rhodamine B was loaded into the core layer of the CMN for visualization and inserted into 2-mm thick pig cadaver skin for analysis of overall insertion quality.

Fig. 3(B) shows the CMN array loaded with rhodamine B inserted into pig cadaver skin, and Fig. 3(C) shows the same CMN array insertion visualized under fluorescence microscopy. Because the CMN array contains a base layer without rhodamine B and a core layer with rhodamine B, the insertion of the CMN array into pig skin results in fluorescence that is separated from the skin surface. The base layer was not visible under fluorescence microscopy, whereas the core layer was represented by a distinct red color. The trace of rhodamine B from the pig cadaver skin depicts the number of microneedles from the patch, as Fig. 3(B) and (C) show 37 red dots as remnants of rhodamine B. However, this was not sufficient to measure the insertion depth of the rhodamine B-loaded CMN array. Therefore, a cross-sectional image of the inserted row was obtained to measure the depth of the CMN core layer (Fig. 3(D)). As rhodamine B was only loaded in the core layer of the CMN, they were located below 250 μm from the surface of the pig cadaver skin. This result indicated that the base layer provided sufficient support to allow deep penetration of the core layer into the skin. Using cryotome sectioning, microneedle insertion depths were further analyzed. As shown in the ESI,† Fig. S2, pig cadaver skin after MP-CMN insertion was sliced at 100 μm thickness, with each slice visualized under a fluorescence microscope. The red dots indicate the core layer with rhodamine B. At 200 μm, only a small portion of the core layer was visible, as the core layer was located at 250 μm above the base layer. Due to the dissolution and diffusion, rhodamine B is visible at lower depth. Similarly, rhodamine B was also visible at a depth of 600 μm. This indicates that M119 will be released from the PLGA microspheres between 200 μm and 600 μm depth, where the core layer is likely to be dissolved post insertion.

OCT imaging was further utilized to observe MP-CMN dissolution in pig cadaver skin. Fluorescence microscopy did not show the dissolution rate of CMN, as rhodamine B was quantified regardless of CMN dissolution. In contrast, OCT imaging enabled the observation of CMN size at different time points. As shown in Fig. 3(E)-(i), MP-CMN images were captured at 5-min intervals to track the shape change post-insertion into the pig cadaver skin. At 15 min, the OCT image showed the remaining MP-CMN base layer (250 μm) (Fig. 3(E)-(ii)). Although MP-CMN insertion analysis suggests robust insertion into the animal skin model, the dissolution of MP-CMN after insertion does not imply an immediate release of the drug captured inside the PLGA microspheres. As M119 is encapsulated by PLGA microspheres, its release is not determined by the dissolution of MP-CMN. Rather, it is determined by the

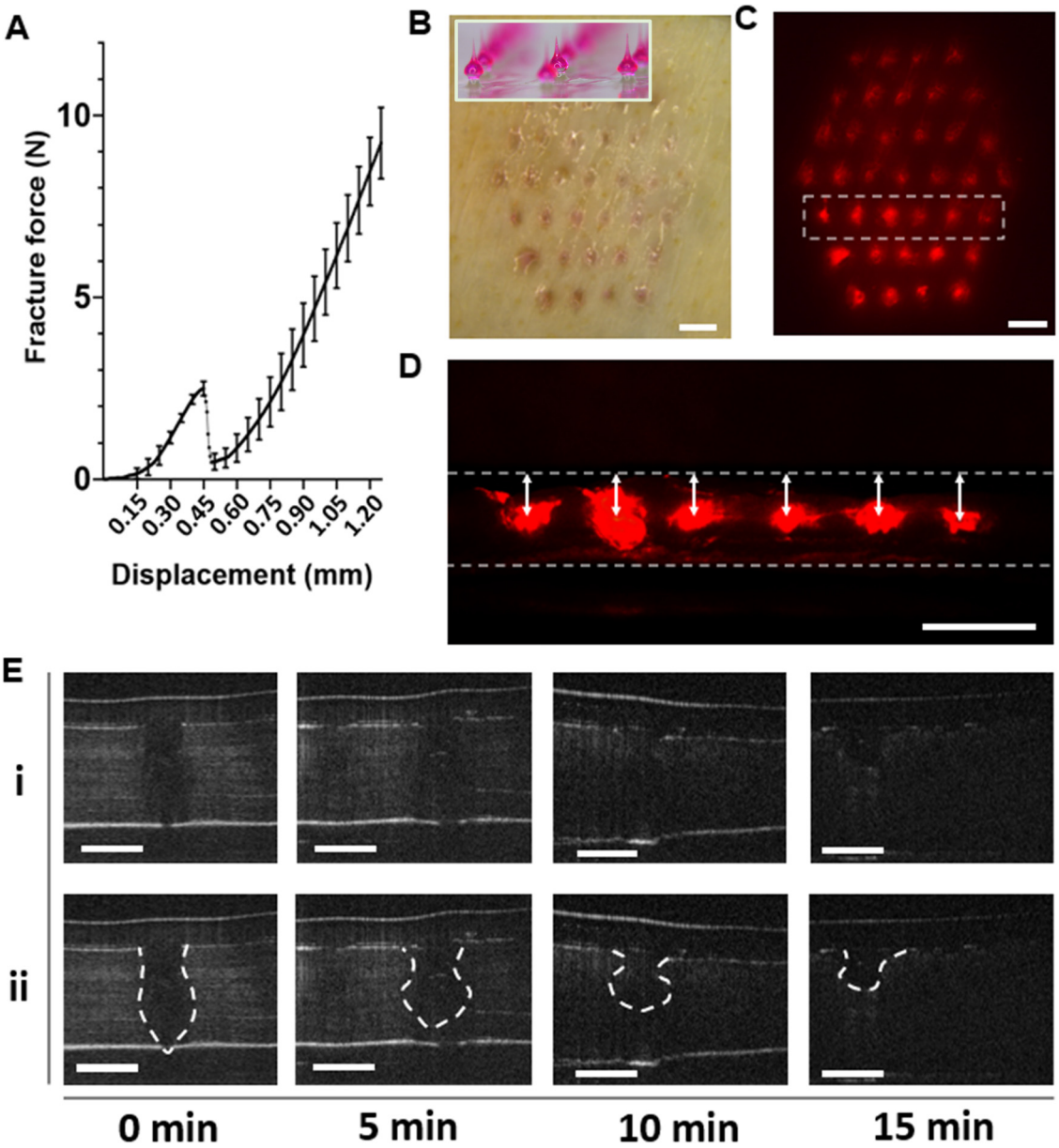

Fig. 3 (A) Fracture force of microneedles on the MP-CMN array (n = 5). (B) Rhodamine B-loaded CMN and insertion into the porcine cadaver skin section (scale bar: 1000 μm). (C) Fluorescence image of rhodamine B-loaded CMN inserted into porcine cadaver skin (scale bar: 1000 μm). (D) A cross-sectional view of porcine cadaver skin after rhodamine B-loaded CMN insertion. (E) Optical coherence tomography of MP-CMN inserted into porcine cadaver skin over time, (i) with a white dashed outline of the CMN geometry and (ii) over 15 min after application at 5-min intervals (scale bar: 500 μm).

degradation of the PLGA microspheres in the core layer. The degradation of M119-encapsulating PLGA microspheres enabled the sustained release of M119, as shown previously. The insertion quality and dissolution of MP-CMN are critical for drug delivery, as PLGA microspheres are transported to delivery targets *via* MP-CMN. However, the insertion was less challenging than that observed in conventional DMN, as the drug-free base layer of the MP-CMN can provide extra space for drug delivery to the core layer. The microneedle residue after the insertion was collected, as the base layer of the MP-CMN is partially dissolved. To check whether the core layer remained intact in the skin even after the microneedle patch was removed, the microneedle residue was measured in height. In the ESI,† Fig. S3, the residual microneedle base layer height level was showcased as a heatmap, each cell indicating a single microneedle post insertion. Overall, the residue had an average remaining height between 250 μm and 300 μm, with few exceptions of MP-CMNs resulting in incomplete insertion.

The *in vitro* insertion data were further correlated with *in vivo* analyses. The efficacy of MP-CMN insertion was evaluated on live C57BL/6 male mice (Fig. 4(A)). Hair quality and skin resilience can contribute to resisting the insertion of microneedles, resulting in incomplete insertion and unsuccessful drug delivery even with sufficient insertion force.[24,27,29,30]

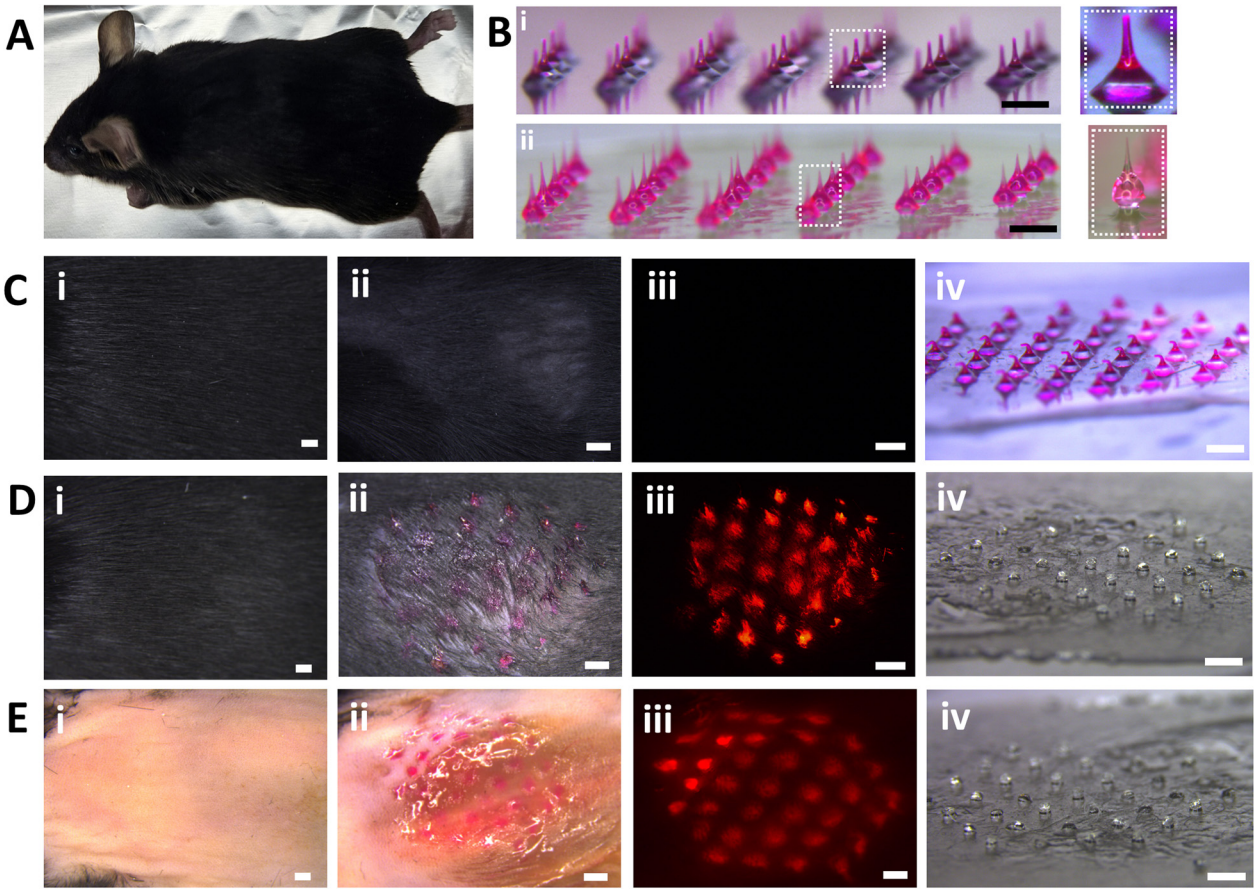

Fig. 4 *In vivo* insertion of rhodamine B-encapsulated CMN in C57BL/6 mice. (A) Image of a 7-week-old C57BL/6 mouse before hair removal. (B) (i) Image of rhodamine B-encapsulated DMNs. (ii) Image of rhodamine B-encapsulated CMNs (scale bar: 1000 μm). (C) Insertion of rhodamine B-encapsulated DMNs into mouse dorsal skin before hair removal. (i) Mouse dorsal skin before hair removal. Image of rhodamine B-encapsulated DMN insertion into mouse dorsal skin before hair removal, as viewed under light (ii) and fluorescence (iii) microscopy. (iv) Rhodamine B-encapsulated DMN patch after 15-min insertion into mouse dorsal skin (scale bar: 1000 μm). (D) Rhodamine B-encapsulated CMN insertion into mouse dorsal skin before hair removal. (i) Mouse dorsal skin before hair removal. Image of rhodamine B-encapsulated CMN insertion into mouse dorsal skin before hair removal, as viewed under light (ii) and fluorescence (iii) microscopy. (iv) Rhodamine B-encapsulated CMN patch after 15-min insertion into mouse dorsal skin (scale bar: 1000 μm). (E) (i) Mouse dorsal skin after hair removal. Image of rhodamine B-encapsulated CMN insertion into mouse dorsal skin after hair removal, as visualized under light (ii) and fluorescence (iii) microscopy. (iv) Rhodamine B-encapsulated CMN patch after 15-min insertion into mouse dorsal skin (scale bar: 1000 μm).

To ensure the MP-CMNs have delivered their drug loading core into the skin, rhodamine B-loaded DMNs and CMNs were inserted into the dorsal skin of live mice before and after hair removal to compare their effectiveness on hairy skin (Fig. 4(B)). The DMN had a clear base with a rhodamine B-encapsulating tip on the top (Fig. 4(B)-(i)). Contrastingly, rhodamine B was excluded from the base layer of the CMN to demonstrate the delivery of the core layer into the dorsal skin of the mice (Fig. 3(D)). Fig. 4(C)-(i) and (D)-(i) show the DMN and CMN insertions on the dorsal skin of unshaven mice. DMN and CMN patches were inserted for 15 min and removed, which were then observed under a light microscope and fluorescence imaging was carried out. As shown in Fig. 4(C)-(ii), only small traces of DMN microneedle patch application were visible, with no indications of rhodamine B. In contrast, distinct characteristics of CMN insertion were observed (Fig. 4(D)-(ii)). Similar to the light microscopy results, fluorescence imaging showed a clear difference between DMN and CMN. No fluorescence was observed following DMN application, suggesting that rhodamine B was not delivered (Fig. 4(C)-(iii)). In contrast, the CMN insertion location was visible, as indicated by red dots under fluorescence microscopy (Fig. 4(C)-(iii)). This contrast was further demonstrated by the observation of the patches 15 min after insertion. Fig. 4(C)-(iv) and D-(iv) show the DMN and CMN patches after application, respectively. All the DMNs had bent ends, demonstrating incomplete insertion due to hair presence on the mouse dorsal skin. There was no sign of rhodamine B on the CMN patch, as the CMNs had dissolved after insertion into the dorsal skin.

CMNs were inserted into the dorsal skin of shaven mice to demonstrate that the presence of hair did not affect their effectiveness. Fig. 4(E)-(i) and (ii) show mouse dorsal skin after hair removal. The dorsal skin was treated with rhodamine B-loaded CMN after hair removal. Fig. 4(E)-(iii) shows the

fluorescence image of CMN insertion on the shaven mouse dorsal skin. As shown in Fig. 4(E)-(iv), the remaining patch showed no trace of rhodamine B, indicating that CMN could deliver a core layer with or without hair removal. As MP-CMN target patient compliance, they must remain effective regardless of the presence of hair. MP-CMN showed a similar insertion effect to CMN (Fig. 4(D)-(iv) and (E)-(iv)), confirming that MP-CMN-induced hair growth does not halt drug administration.

Efficacy of MP-CMN *in vivo*

The *in vivo* efficacy of MP-CMN was evaluated in 7-week-old male C57BL/6 mice, as they exhibit telogen phase lasting between postnatal day 42 and 53.[31,32] This will allow the comparative evaluation of the hair growth-promoting effect of vasodilator M119. Also, this will confirm the effective microneedle insertion even in the presence of regrown hair that might otherwise obstruct penetration. Five experimental groups were used (n = 4 per group), and the dorsal skin of each mouse was shaved. The negative control group received no treatment for 28 days, and the positive control group received topical application of 2% w/v minoxidil once every other day; this drug is widely used in alopecia research.[33] Previous research has shown that topical application of M119 exhibited a similar hair growth effect when compared with topical application of minoxidil.[19] Still, topical M119 application required twice administrations daily. The vehicle control group was administered CMN loaded with blank PLGA microspheres. The single and double MP-CMN application groups each received MP-CMN that contained M119 in PLGA microspheres. The single application group received MP-CMN on day 0 whereas the double application group received two applications of MP-CMN, one on day 0 and a second one on day 14 (Fig. 5(A)). Hair growth was recorded on days 1, 7, 14, 21, and 28. Images of mice from each experimental group are shown in Fig. 5(B), and images of all mice used in this experiment are shown in the ESI,† Fig. S1.

On day 7, all groups except the negative control group showed visual signs of hair growth, whereas the vehicle control showed limited hair recovery. Moreover, the single- and double-application groups had a broader hair recovery area than that of the vehicle control group (Fig. 5(B)). Day 14 hair conditions were similar to those on day 7; the negative control group showed almost no signs of hair growth, except for the outer edges of the dorsal area. Contrastingly, the vehicle group showed hair growth on a small area of skin near the microneedle application site. On day 21, both the positive and single-application groups showed similar hair growth. The MP-CMN double application group had a denser hair concentration compared to the other groups because these mice received

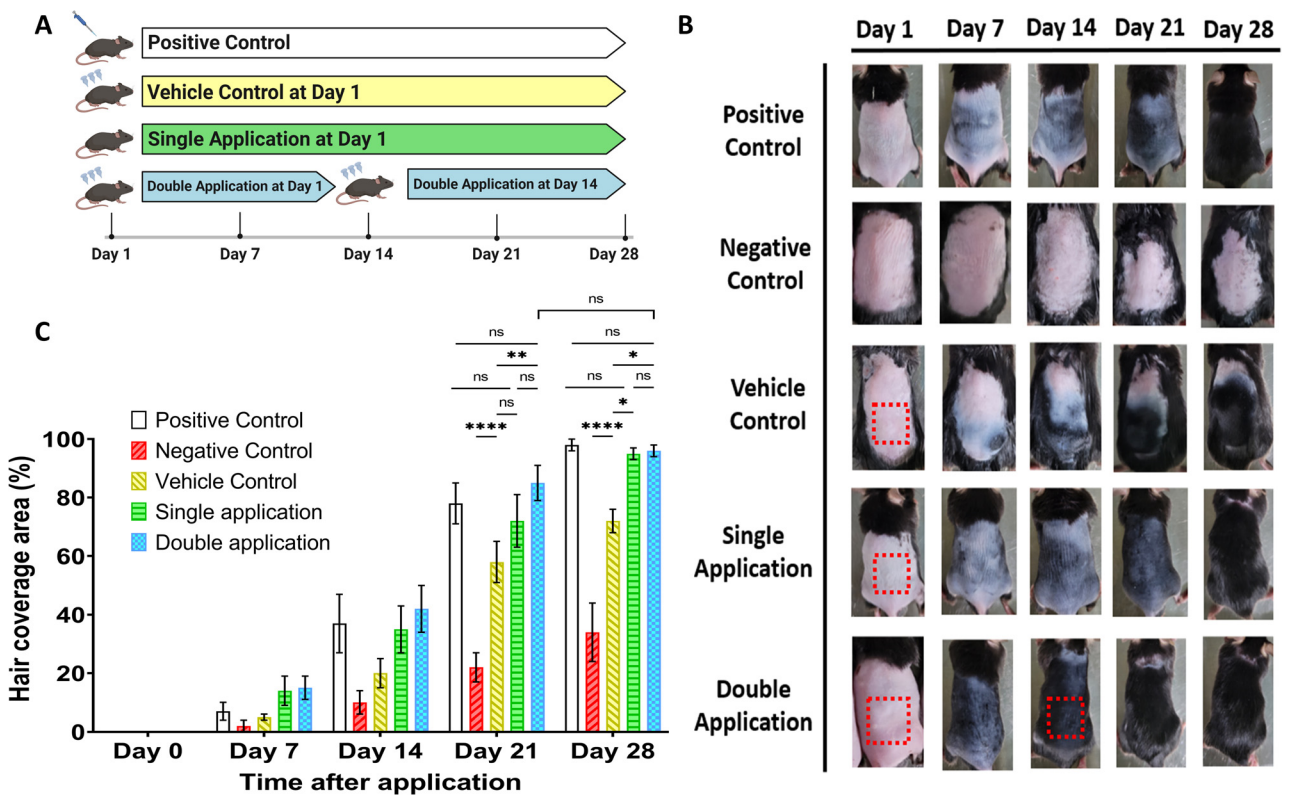

Fig. 5 A comparative result of hair growth efficacy of MP-CMN. (A) Schematic representation of the *in vivo* experimentation outline. (B) *In vivo* results of mice after experimentation. Images of the mouse dorsal skin area were taken on days 1, 7, 14, 21, and 28. The red box represents the size of CMN patches that were applied onto the mouse. H&E staining analysis of hair follicle and hair growth after *in vivo* experimentation is also shown on the right. (C) The hair coverage area of the mouse dorsal skin was analyzed by measuring the density of hair on days 1, 7, 14 and 28. The results are shown as mean ± SD from measurements in N = 4 mice.

additional MP-CMN administration on day 14, which enhanced the hair growth (Fig. 5(B)). The vehicle control group also showed a portion of the dorsal skin covered with hair and hairless parts. However, the hairless areas were not sites of microneedle application, which can affect hair growth. The minoxidil positive control, MP-CMN single application, and double application groups recovered their original hair condition on day 28. In contrast, the MP-CMN double application group showed no visible difference from day 21, with the fastest recovery compared to the other groups (Fig. 5(B)).

The area of hair regrowth was measured by calculating the blackened area from the previous stage using an image contrast analysis tool (Fig. 5(C)). Positive control and both single and double applications showed the highest hair recovery of 98.1 ± 1.9%, 94.7 ± 2.1%, and 95.6 ± 2.0%, respectively, on day 28. The vehicle control showed a notably high hair recovery area of 72.1% ± 4.1% on day 28, that occurred despite the absence of active M119 in the applied CMN. While this outcome was significantly lower than that observed with M119, it still demonstrated a substantial regenerative effect. For comparison, in the negative control group (without any treatment) hair recovery amounted to 34.5 ± 9.5% at day 28. The experimental group treated with CMN containing only PLGA microspheres was included for the analysis of possible hair growth effects from PLGA, as lactate degraded from PLGA has been previously reported to induce angiogenesis.[34–36] Vehicle control, MN loading only PLGA microspheres, exhibited 73.4% effectiveness when compared to the positive control. Similarly, it exhibited 76.5% and 75.3% effectiveness compared to single and double applications. Although the vehicle control showed less effectiveness than topical minoxidil or MP-CMN, PLGA microspheres may have induced some angiogenic factors in the mice, consequently enhancing the regrowth of hair follicles (Fig. 5(C)).

The MP-CMN single- and double-application groups showed similar hair growth overall, whereas the MP-CMN double-application group showed more hair growth after the second MP-CMN application on day 14. On day 28, the difference was negligible. On day 21, the hair coverage area following double application of MP-CMN was 1.46-fold higher than the vehicle control (CMN with PLGA microsphere only) which was significant. On the other hand, at day 21 the difference between the hair coverage area following double *versus* single application of MP-CMN was not significant (Fig. 5(C)). It was also noteworthy that the hair coverage area between the vehicle control and single application group had no significant differences until day 21. Although the difference grows as the time passes to day 28, it is still remarkable that the PLGA microsphere CMNs show outcomes that can potentially have more effects with an appropriate administration strategy.

On day 28, there were no significant differences between the MP-CMN single- and double-application groups. This suggests that a single MP-CMN application can be used once every 28 days for alopecia treatment, indicating a potential improvement in patient compliance with a single monthly application. Moreover, because MP-CMNs can be applied to hair-grown skin, they can be used for continuous treatment after 28 days, even for months.

The histology of mouse dorsal skin cross-sections was analyzed using H&E staining after 28 days. The mouse dorsal skin was excised and cut laterally and longitudinally to locate the sectional cut of hair and measure skin thickness (Fig. 6(A)). Fig. 6(B) shows the cross-section of the mouse dorsal skin on the lateral and longitudinal sides for the experimental groups. The cross-section of hair in the skin epidermal area is marked with a black arrow (Fig. 6(B)). Fig. 6(C) shows the average skin thickness in each group, as measured from excised skin. The negative control had a mean thickness of 305.13 ± 66.08 μm, which was significantly lower than other experimental groups. The positive control, vehicle control, single administration, and double administration groups had mean thicknesses of 703.13 ± 59.02, 542.12 ± 40.87, 655.47 ± 46.85, and 643.46 ± 51.46 μm, respectively. No significant differences were observed between these groups, other than the comparison between positive control and vehicle control. These results support the hair recovery data, where the positive control, single administration, and double administration groups had similar hair growth on day 28 (Fig. 5(C)). Because a single administration showed similar results to double administration, it can be concluded that a single MP-CMN administration every 28 days is as potent as two administrations and every other day topical minoxidil administration. A previous study on M119 microneedles showed that the microneedle experimental group had the thickest skin[19] which may be inconsistent with the results observed in the present study where an only non-significant trend favoring MP-CMN over vehicle control to increase skin thickness was observed. This inconsistency could be explained by the number of microneedles applied. Prior studies performed microneedle application every other day, whereas in the present study applications were once per two weeks. This may have resulted in differences in skin thickness, as multiple applications of microneedles can increase epidermal integrity and dermal thickness.[37] The number of hairs was then counted to obtain the average number of lateral and longitudinal hair cross-sections per mm (Fig. 6(D)), and MP-CMN single administration and double administration groups had an average lateral hair per mm of 66.8 ± 4.1, 54.2 ± 3.9 and 55.6 ± 2.9, respectively. Moreover, the vehicle control had a thickness of 542.12 ± 40.87 and lateral hair per mm of 26.4 ± 7.1, both of which were significantly lower than those of the minoxidil positive control, as well as the MP-CMN single administration and double administration. Still, the vehicle control showed comparatively more hair growth indicators than the negative control, which highlights the potential CMN with PLGA microsphere for alopecia treatment.

MP-CMN application resulted in hair growth in mouse models. The level of hair regeneration was the highest when MP-CMNs were used. Single and double applications of MP-CMNs showed similar results on day 28, although the double-application group showed an enhanced effect on day 21. MP-CMNs also proved to be applicable to hairy skin, as shown in Fig. 4(D), demonstrating that MP-CMNs can be applied in long and repetitive treatments despite continuous hair growth throughout treatment. The vehicle control, which was treated with CMNs

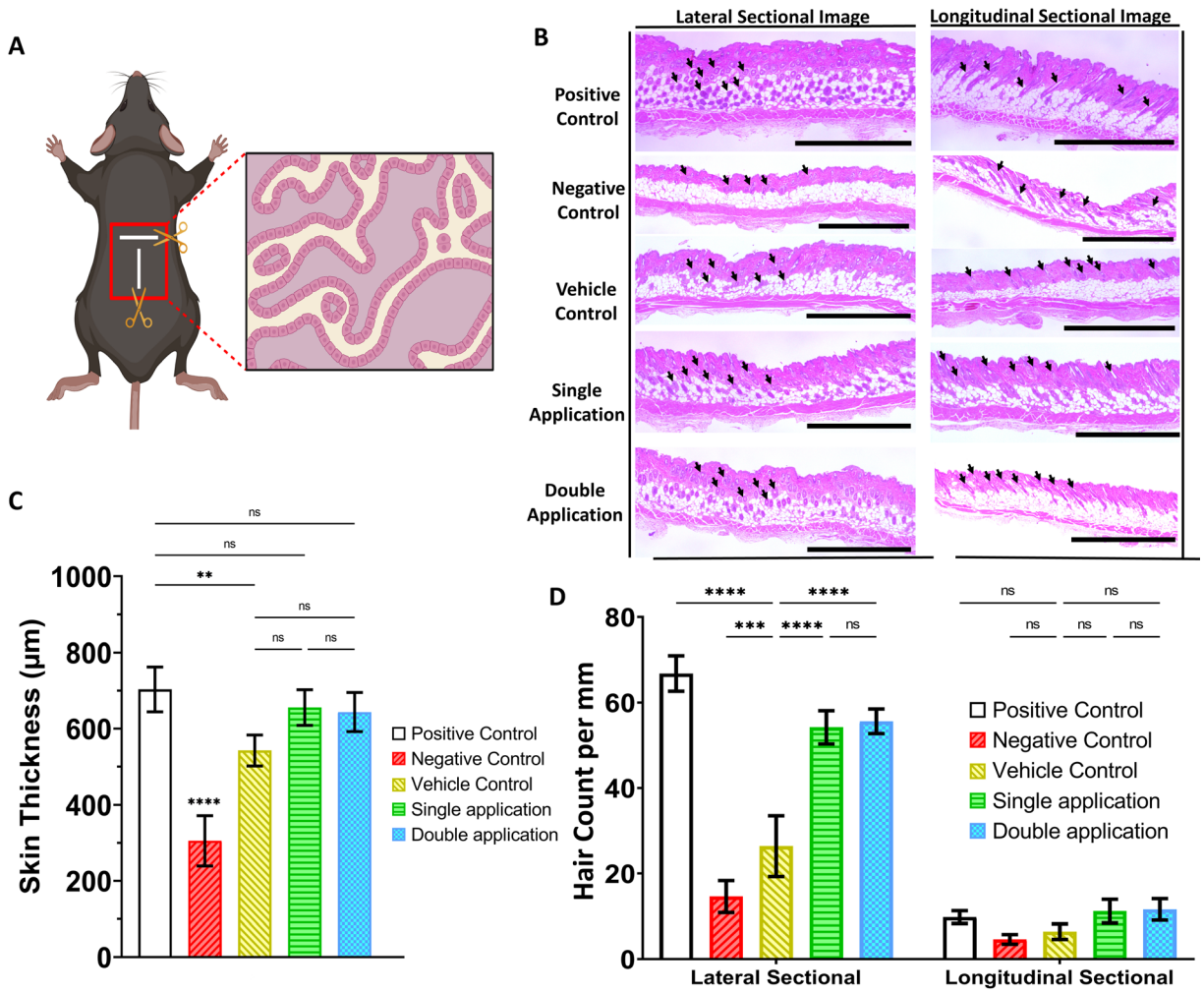

Fig. 6 H&E staining analysis of mouse dorsal skin excision. (A) A schematic image of the lateral and longitudinal excision and cross-sectional view of mouse skin. (B) H&E staining results for both the lateral and longitudinal sections of mouse dorsal skin (scale bar: 1000 μm). (C) Hair thickness measurement from mouse dorsal hair after day 28. (D) Number of hairs per mm of both the lateral and longitudinal section. Results in C and D are depicted as means ± SD from N = 4 mice.

containing PLGA microspheres without drug encapsulation, exhibited hair regenerative effects. Overall, MP-CMNs may be an effective alopecia treatment method. In the present study, M119 with PLGA microspheres had potent effects on hair growth, with CMN acting as a platform for scalp delivery.

Experimental

Preparation of M119-loaded and blank PLGA microspheres

In a beaker, 90 mL of 1% Tris hydrochloride buffer-polyvinyl alcohol solution was stirred at 700 rpm. A beaker containing 200 mg PLGA (50 : 50 lactide : glycolide ratio) and 10 mg M119 was precooled on ice for 5 min. Next, 1 mL of ice-cold dichloromethane was transferred to the precooled beaker and mixed for 2 min at 20 000 rpm using a homogenizer. Then, 10 mL of 1% Tris hydrochloride buffer-polyvinyl alcohol solution was added and stirred for 2 min at 20 000 rpm using a homogenizer. Immediately after mixing, the solution was transferred to a second beaker containing 90 mL of 1% Tris hydrochloride buffer-polyvinyl alcohol solution. The dichloromethane was subsequently evaporated for 18 h while the solution was stirred on a magnetic stirrer at 700 rpm. Next, the PLGA microsphere aqueous suspension was washed thrice with ultrapure water, and the formed microspheres were collected through centrifugation at 1607 × g. The PLGA microsphere-containing flask was attached to a rotation evaporator and cooled to −80 °C. This process was terminated when the microsphere suspension froze on the surface of the flask. The frozen microsphere mixture was stored in a −80 °C freezer for 30 min and dried for 24–48 h. The PLGA microspheres were then stored at −20 °C. PLGA microspheres without M119 encapsulation were prepared using 200 mg PLGA (50 : 50 lactide : glycolide ratio), similar to the preparation of the M119-loaded PLGA microspheres.

Microsphere M119 encapsulation analysis

A laser diffractometer (Helos H1964 PSD; Sympatec, Clausthal-Zellerfeld, Germany), Helos software, and 6 mL Cuvette Sympatec

Helos (Sympatec) were used to measure the size and particle scattering diffusometry of the PLGA microspheres. The measurements were carried out with the Helos R1 (range, 0.1–35 μm) and R3 (range, 0.9–175 μm) lenses. The dried PLGA microspheres were dispersed in water containing 0.1% Tween-80 and placed in an ultrasonic bath for 1 min. Each sample was measured thrice, and the average of these measurements was recorded. The mean particle diameter (×50) was used as the main value of the particle sizes. Two milligrams of dried PLGA microspheres were dissolved in 1 mL of acetonitrile, diluted, and measured using liquid chromatography–mass spectrometry (LC–MS).

In vitro release assay of M119-loaded PLGA microspheres

Simulated interstitial fluid (SISF) buffer (1 mL) supplemented with 117 mM NaCl, 3 mM KCl, 2.8 mM $CaCl_2 \times 2H_2O$, 1 mM $MgCl_2$, 27 mM $NaHCO_3$, 0.5 mM Na_2SO_4, and 1 mM K_2HPO_4 was mixed 1 : 1 with human blood plasma and normocin at a concentration of 1 : 500. Dried M119 PLGA microspheres (5 mg) were placed in the donor chamber of a rapid equilibrium dialysis (RED) assay plate. The donor chamber was filled with the maximum volume of phosphate-buffered saline (500 μL). The SISF buffer solution, spiked with the internal deuterated standard M119, was added to the receiver chamber. The maximum filling volume was 750 μL. The RED plate was then sealed with an aluminum foil seal, incubated at 37 °C and shaken at 200 rpm; the release profile was monitored during this period. The receiver chamber was filled with a fresh SISF buffer solution for sampling. The samples were stored at −20 °C until the last day of sampling (day 29). They were then thawed at room temperature for 60 min for LC–MS analysis using solid-phase extraction (protein precipitation Sirocco plate; Waters, Milford, MA, USA). M119 in the human blood plasma-SISF buffer solution was quantified using a calibration curve with a deuterated internal standard. A calibration curve was prepared at six calibration concentrations: 0.1, 0.5, 1.0, 5.0, 10, 25, and 50 nM, each of which was spiked with 1 nM deuterated M119 as the internal standard.

LC–MS analysis

LC–MS was performed using an Agilent 1100 quaternary pump mass spectrometer (API 4000 LC/MS/MS Triple Quad.; AB Sciex, Framingham, MA, USA) with an injection volume of 25 μL and a flow rate of 400 μL min^{-1} using a high-performance liquid chromatography column (ACE UltraCore 2.5 SuperC18 50 × 2.1 mm; Avantor, Radnor, PA, USA). The column oven temperature was set to 40 °C. The mobile phase gradient was made using (1) solvent A: acetonitrile and MeOH at 50 : 50 v/v ratio, 0.1% fumaric acid, and 2 mM ammonium formate; and (2) solvent B: water, 0.1% fumaric acid, and 2 mM ammonium formate. The gradient was created as shown in Table 1.

Table 1 Gradient solvent ratio

Time (Min)	Solvent A (%)	Solvent B (%)
1.50	70	30
2.00	5	95
5.00	5	95
5.50	95	5
6.20	95	5
6.50	70	30

MP-CMN fabrication

An MP-CMN is composed of a base, core, and tip, which require distinct assembly methods. The base was made by dispensing 60% w/v pharmaceutical-grade hyaluronic acid (PHA, 30 kDA; Uscarepharm, Suwon, Republic of Korea) aqueous solution on a polyurethane patch. A plate cover was then placed on top of the dispensed solution, with a 250-μm gap between the patch and cover. Hyaluronic acid stayed connected with the plate, forming an hourglass shape as the solution droplets dried. The core solution was then formulated by mixing 60% w/v PHA and 1.84% w/w M119-encapsulating PLGA microsphere (TOPADUR, Zurich, Switzerland) and dispensed on top of the dried base. Next, the tip of the MP-CMN was fabricated by mixing 30% w/v PHA solution and dispensing it on top of the core, followed by centrifugal lithography at 250 × *g* for 30 s. The final MP-CMN contains 0.79 μg M119 per MP-CMN array; each array contains 37 MP-CMNs in total.

Preparation of topical minoxidil solution

A topical minoxidil formulation was produced to compare its efficacy on hair growth with that of MP-CMN. The formulation was prepared with polyethylene glycol 400 (Sigma-Aldrich, St. Louis, MO, USA) and ethanol (99.5°; Sigma-Aldrich) mixed in a 50 μL solution at a ratio of 7 : 3 v/v. Minoxidil (Sigma-Aldrich) was further mixed in the solution at a ratio of 2% w/v. The topical formulation (50 μL) was subsequently administrated to the experimental group at two-day intervals.

MP-CMN morphological analysis

The MP-CMN's morphological characteristics were visualized using a bright-field microscope (M165 FC; Leica, Wetzlar, Germany). The height, width, and tip diameter of the MP-CMNs were subsequently measured. Furthermore, their mechanical strength was measured using a force analyzer (Z0.5TN; Zwick/Roell Inc., Ulm, Germany). The probe of the force analyzer measured the vertical axial strength of the MP-CMN by pressing the microneedle at a vertical velocity of 3.0 mm min^{-1}. The skin penetration ability and insertion depth of MP-CMN was evaluated by applying it to porcine cadaver skin (Cronex, Hwaseong, Korea) and analyzing sectional cuts using optical coherence tomography (OQ StrataScope 1.0; Lumedica, Durham, NC, USA). An ion beam cross section polisher (IB-19510CP; JEOL, Tokyo, Japan) was used to cut the MP-CMN for cross section observation. Scanning electron microscopic (SEM) images of the section-cut MP-CMNs were obtained using an FE-SEM (JEOL-7800F; JEOL, Tokyo, Japan).

Hair growth mouse model and ethical approval

Animal experiments were conducted in accordance with the ethical guidelines and regulations of the Yonsei Laboratory Animal Research Center. All procedures were approved by the Institutional Animal Care and Use Committee of Yonsei

University (Approval Number: IACUC-202302-1646-03). Six-week-old male C57BL/6 mice (Orient Bio, Seongnam, Republic of Korea) were acclimated for one week. Then, the dorsal skin area of the 7-week-old mice was shaved. In the experimental groups, mice were treated with topical minoxidil solution (positive control), no treatment (negative control), CMNs with PLGA microspheres encapsulating no drug (vehicle control), or MP-CMNs (single and double administration). 4 mice were present in each group. Positive control mice were treated with a minoxidil topical solution every two days for 28 days. Single-administration mice were treated with MP-CMN on day 1, whereas double-administration mice were treated with MP-CMN on days 1 and 14. All mice were housed at room temperature (22–24 °C) with a 12 h light and dark cycle. The dorsal area of each mouse was analyzed to observe the hair growth using an image analysis program (ImageJ; National Institutes of Health, Bethesda, MD, USA). The hair growth was analyzed by measuring and comparing the area of hair covering the dorsal hair, every 7 days.

Histological staining

Mouse skin tissues were excised from the dorsal area and fixed overnight in 4% (w/v) paraformaldehyde (Sigma-Aldrich). The tissues were cut into 10-μm thick slices, which were then stained with hematoxylin and eosin (H&E) to evaluate skin thickness and hair regeneration. The stained slices were observed under a bright-field microscope (M165 FC; Leica).

Statistical analysis

All data are expressed as the mean ± standard deviation. Statistical analyses were performed using Student's *t*-test or analysis of variance through GraphPad Prism (version 6.0; GraphPad Software Inc., Boston, MA, USA). The results were obtained from four or more groups. Statistical significance was set at $p < 0.05$ ($^{*}p < 0.05$, $^{**}p < 0.01$, and $^{***}p < 0.001$).

Conclusions

Our study indicates that the use of PLGA to encapsulate M119, a NO-releasing PDE5 inhibitor and highly effective vasodilator drug for hair growth, may facilitate sustained drug release to effectively treat alopecia. The monthly application of this treatment could improve patient compliance. *In vitro* and *in vivo* analyses demonstrated successful MP-CMN penetration in the skin of an animal model, as well as delivery of M119-encapsulating PLGA microspheres to hair follicles to promote hair regrowth. Our study showed that microneedles act as a tool for skin penetration and delivery, whereas sustained release is achieved through loaded microspheres that capture drugs. Thus, the use of MP-CMN could mitigate the limitations of previous alopecia treatments that utilize DMN, such as frequent administration and low drug efficacy due to the skin barrier. Additionally, the possibility of using PLGA as a hair growth agent was examined, which showed good efficacy. However, the substantial hair regrowth effect of this polymer warrants further study. The effect of the sustained release of PLGA microspheres and the drug delivery of the CMN system could be utilized for multiple drugs. Therefore, they could be applied in the treatment of different diseases.

Author contributions

J. S., Y. K., G. K., R. N., and H. J. conceptualization of study. J. S., S. C., T. B., and H. T. data curation and investigation. J. S., Y. K., T.B., and H. T. methodology and visualization. H. T., C. L., R. N., and H. J. validation. J. S., S. C., T. B., and C. L. writing – original draft. J. S., S. C., T. B., and C. L. writing – reviewing and editing. C. L., R. N., and H. J. funding acquisition and supervision. R. N., and H. J. Project administration.

Data availability

Data supporting this article have been included as part of the ESI.†

Conflicts of interest

Hyungil Jung is an inventor of patents that have been or may be licensed to JUVIC Inc. and is a founder and shareholder of JUVIC Inc., developing microneedle-based products. Reto Naef is a founder of TOPADUR Pharma AG. Tobias Braun, Hermann Tenor, Christian Ludin are employees of TOPADUR Pharma AG. These potential conflicts of interest have been disclosed by Yonsei University.

Acknowledgements

This research was supported by a grant of the Korean Health Technology R&D Project through the Korea Health Industry Development Institute (KHIDI), funded by the Ministry of Health & Welfare, Republic of Korea (grant number: RS-2023-00266598). It is also financially supported by the Ministry of Trade, Industry and Energy (MOTIE) and Korea Institute for Advancement of Technology (KIAT) through the International Cooperative R&D program (grant number: P0026099). It is also supported by the Korea Institute for Advancement of Technology (KIAT) funded by the Ministry of Trade, Industry and Energy in 2024 (grant number: RS-2024-00418203). It is also supported in part by the Brain Korea 21 (BK21) FOUR program.

References

1 T. G. Phillips, W. P. Slomiany and R. Allison, Hair Loss: Common Causes and Treatment, *Am. Fam. Physician*, 2017, **96**, 371–378.
2 S. Heilmann-Heimbach, C. Herold, L. M. Hochfeld, A. M. Hillmer, D. R. Nyholt, J. Hecker, A. Javed, E. G. Chew, S. Pechlivanis, D. Drichel, X. T. Heng, R. C. Del Rosario, H. L. Fier, R. Paus, R. Rueedi, T. E. Galesloot, S. Moebus, T. Anhalt, S. Prabhakar, R. Li, S. Kanoni, G. Papanikolaou, Z. Kutalik, P. Deloukas, M. P. Philpott, G. Waeber,

T. D. Spector, P. Vollenweider, L. A. Kiemeney, G. Dedoussis, J. B. Richards, M. Nothnagel, N. G. Martin, T. Becker, D. A. Hinds and M. M. Nothen, Meta-analysis identifies novel risk loci and yields systematic insights into the biology of male-pattern baldness, *Nat. Commun.*, 2017, **8**, 14694.

3 C. X. Yap, J. Sidorenko, Y. Wu, K. E. Kemper, J. Yang, N. R. Wray, M. R. Robinson and P. M. Visscher, Dissection of genetic variation and evidence for pleiotropy in male pattern baldness, *Nat. Commun.*, 2018, **9**, 5407.

4 N. Hunt and S. McHale, The psychological impact of alopecia, *Br. Med. J.*, 2005, **311**, 951–953.

5 D. Williamson, M. Gonzalez and A. Y. Finlay, The effect of hair loss on quality of life, *J. Eur. Acad. Dermatol. Venereol.*, 2001, **15**, 137–139.

6 A. K. Gupta, M. Talukder, M. Venkataraman and M. A. Bamimore, Minoxidil: a comprehensive review, *J. Dermatol. Treat.*, 2022, **33**, 1896–1906.

7 A. K. Gupta, M. Venkataraman, M. Talukder and M. A. Bamimore, Finasteride for hair loss: a review, *J. Dermatol. Treat.*, 2022, **33**, 1938–1946.

8 M. S. Alqahtani, M. Kazi, M. A. Alsenaidy and M. Z. Ahmad, Advances in Oral Drug Delivery, *Front. Pharmacol.*, 2021, **12**, 618411.

9 S. Kim, J. Eum, H. Yang and H. Jung, Transdermal Finasteride Delivery *via* Powder-carrying Microneedles with a Diffusion Enhancer to Treat Androgenetic Alopecia, *J. Controlled Release*, 2019, **316**, 1–11.

10 M. S. Irwig, Persistent Sexual Side Effects of Finasteride: Could They Be Permanent?, *J. Sex. Med.*, 2012, **9**, 2927–2932.

11 R. Sanz, A. C. Calpena, M. Mallandrich and B. Clares, Enhancing Topical Analgesic Administration: Review and Prospect for Transdermal and Transbuccal Drug Delivery Systems, *Curr. Pharm. Des.*, 2015, **21**, 2867–2882.

12 A. Therianou, C. Vincenzi and A. Tosti, How safe is prescribing oral minoxidil in patients allergic to topical minoxidil?, *J. Am. Acad. Dermatol.*, 2022, **86**, 429–431.

13 A. Goren and T. Naccarato, Minoxidil in the Treatment of Androgenetic Alopecia, *Dermatol. Ther.*, 2018, **31**, 12686.

14 A. Rossi, C. Cantisani, L. Melis, A. Iorio, E. Scali and S. Calvieri, Minoxidil Use in Dermatology, Side Effects and Recent Patents, *Recent Pat. Inflammation Allergy Drug Discovery*, 2012, **6**, 130–136.

15 Z. Sartawi, C. Blackshields and W. Faisal, Dissolving microneedles: Applications and growing therapeutic potential, *J. Controlled Release*, 2022, **348**, 186–205.

16 D. AlSaad, B. H. Lee and S. Al-Obaidly, Finasteride Use During Pregnancy and Early Neonatal Outcome: A Case Report, *Int. J. Clin. Pharm.*, 2018, **40**, 803–805.

17 E. A. Olsen, E. R. DeLong and M. S. Weiner, Long-term Follow-up of Men with Male Pattern Baldness Treated with Topical Minoxidil, *J. Am. Acad. Dermatol.*, 1987, **16**, 688–695.

18 L. Rudnicka, M. Arenbergerova, R. Grimalt, D. Ioannides, A. C. Katoulis, E. Lazaridou, M. Olszewska, Y. S. Ovcharenko, B. M. Piraccini, A. Prohic, A. Rakowska, P. Reygagne, M. A. Richard, R. O. Soares, M. Starace, S. Vañó-Galvan and A. Waskiel-Brunat, European expert consensus statement on the systemic treatment of alopecia areata, *J. Eur. Acad. Dermatol. Venereol.*, 2024, **38**, 631–632.

19 Y. Kim, Y. C. Ryu, H. S. Min, H. Yang, J. Nam, C. Lee, D. J. Um, M. Kim, P. Atzei, R. B. Francisco, R. Naef, K.-Y. Choi and H. Jung, Dual-Mode Vasodilator M119 Delivery to Hair Follicle *via* Dissolving Microneedle for Advanced Alopecia Treatment, *Adv. Ther.*, 2022, **5**, 2200052.

20 S. F. Lahiji and Y. Kim, Tissue interlocking dissolving microneedles for accurate and efficient transdermal delivery of biomolecules, *Sci. Rep.*, 2019, **9**, 7886.

21 F. Danhier, E. Ansorena, J. M. Silva, R. Coco, A. L. Breton and V. Préat, PLGA-based Nanoparticles: An Overview of Biomedical Applications, *J. Controlled Release*, 2012, **161**, 505–522.

22 L. K. Vora, R. F. Donnelly, E. Larrañeta, P. González-Vázquez, R. R. S. Thakur and P. R. Vavia, Novel Bilayer Dissolving Microneedle Arrays with Concentrated PLGA Nano-microparticle for Targeted Intradermal Delivery: Proof of Concept, *J. Controlled Release*, 2017, **265**, 93–101.

23 M. Yin, Y. Zeng, H.-Q. Liu, W. Zhang, C. Wang, C. Chen and W. Li, Dissolving Microneedle Patch Integrated with Microspheres for Long-Acting Hair Regrowth Therapy, *ACS Appl. Mater. Interfaces*, 2023, **15**, 17532–17542.

24 H. Tohmyoh, K. Fujita, H. Suzuki and K. Futada, Structural elasticity for tensile deformation of a single human hair and the comparison with it for the bending deformation, *J. Mech. Behav. Biomed. Mater.*, 2021, **113**, 104166.

25 P. Makvandi, M. Kirkby, A. R. J. Hutton, M. Shabani, C. K. Y. Yiu, Z. Baghbantaraghdari, R. Jamaledin, M. Carlotti, B. Mazzolai, V. Mattoli and R. F. Donnelly, Engineering Microneedle Patches for Improved Penetration: Analysis, Skin Models and Factors Affecting Needle Insertion, *Nano-Micro Lett.*, 2021, **13**, 93.

26 R. D. Price, M. G. Berry and H. A. Navsaria, Hyaluronic acid: the scientific and clinical evidence, *J. Plast Reconstr. Aesthet. Surg*, 2007, **60**, 1110–1119.

27 H. S. Min, Y. Kim, J. Nam, H. Ahn, M. Kim, G. Kang, M. Jang, H. Yang and H. Jung, Shape of Dissolving Microneedles Determines Skin Penetration Ability and Efficacy of Drug Delivery, *Biomater. Adv.*, 2023, **145**, 213248.

28 P. Makvandi, M. Kirkby, A. R. J. Hutton, M. Shabani, C. K. Y. Yiu, Z. Baghbantaraghdari, R. Jamaledin, M. Carlotti, B. Mazzolai, V. Mattoli and R. F. Donnell, Engineering Microneedle Patches for Improved Penetration: Analysis, Skin Models and Factors Affecting Needle Insertion, *Nano-Micro Lett.*, 2021, **13**, 93.

29 E. Cloete, N. P. Khumalo and M. N. Ngoepe, Understanding Curly Hair Mechanics: Fiber Strength, *J. Invest. Dermatol.*, 2020, **140**, 113–120.

30 W. Martanto, J. S. Moore, T. Couse and M. R. Prausnitz, Mechanism of fluid infusion during microneedle insertion and retraction, *J. Controlled Release*, 2006, **112**, 357–361.

31 W. H. Wang, R. Ramos, K. Y. Tai, Y. S. Wu, T. Y. Chang, J. Y. Yan, M. V. Plikus, J. W. Oh and S. J. Lin, Studying Hair Growth Cycle and its Effects on Mouse Skin, *J. Invest. Dermatol.*, 2023, **143**, 1638–1645.

32 Q. Wang, J. W. Oh, H. L. Lee, A. Dhar, T. Peng, R. Ramos, C. F. Guerrero-Juarez, X. Wang, R. Zhao, X. Cao, J. Le, M. A. Fuentes, S. C. Jocoy, A. R. Rossi, B. Vu, K. Pham, X. Wang, N. M. Mali, J. M. Park, J. H. Choi, H. Lee, J. M. D. Legrand, E. Kandyba, J. C. Kim, M. Kim, J. Foley, Z. Yu, K. Kobielak, B. Andersen, K. Khosrotehrani, Q. Nie and M. V. Plikus, A multi-scale model for hair follicles reveals heterogeneous domains driving rapid spatiotemporal hair growth patterning, *eLife*, 2017, **6**, 1–97.

33 D. Monti, S. Tampucci, S. Burgalassi, P. Chetoni, C. Lenzi, A. Pirone and F. Mailland, Topical Formulations Containing Finasteride. Part I: *In Vitro* Permeation/Penetration Study and In Vivo Pharmacokinetics in Hairless Rat, *J. Pharm. Sci.*, 2014, **103**, 2307–2314.

34 O. Trabold, S. Wagner, C. Wicke, H. Scheuenstuhl, M. Z. Hussain, N. Rosen, A. Seremetiev, H. D. Becker and T. K. Hunt, Lactate and oxygen constitute a fundamental regulatory mechanism in wound healing, *Wound Repair Regen.*, 2003, **11**, 504–509.

35 A. Flores, S. Choi, Y. C. Hsu and W. E. Lowry, Inhibition of pyruvate oxidation as a versatile stimulator of the hair cycle in models of alopecia, *Exp. Dermatol.*, 2021, **30**, 448–456.

36 J. Ye, X. Tang, Y. Long, Z. Chu, Q. Zhou and B. Lin, The effect of hypoxia on the proliferation capacity of dermal papilla cell by regulating lactate dehydrogenase, *J. Cosmet. Dermatol.*, 2021, **20**, 684–690.

37 B. S. Atiyeh, O. A. Ghanem and F. Chahine, Microneedleing: Percutaneous Collagen Induction (PCI) Therapy for Management of Scars and Photoaged Skin – Scientific Evidence and Review of the Literature, *Aesthetic Plast. Surg.*, 2021, **45**, 296–308.